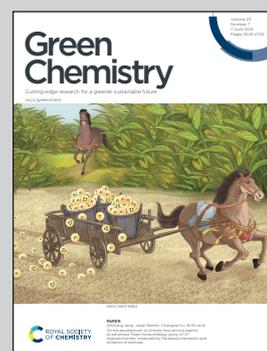Showcasing research from Profs. Sung Yeon Hwang, Jeyoung Park, Dongyeop X. Oh, and co-workers, Research Center for Bio-based Chemistry, KRICT, Ulsan, Republic of Korea.

Sustainable, self-cleaning, transparent, and moisture/oxygen-barrier coating films for food packaging

Functional food packaging has health and environmental issues. Herein, self-cleaning and gas barrier coating films are prepared by using naturally abundant raw materials. A spray-assisted layer-by-layer assembly of cellulose nanofibers and chitosan nanowhiskers coated on one side of the film decreases oxygen transmission rate. A porous surface of silica nanoparticles and chitosan nanowhiskers impregnated with oil on the other side of the film repels the contaminants and exhibits a low water vapor transmission rate.

ROYAL SOCIETY OF **CHEMISTRY**

rsc.li/greenchem

Check for updates

Sustainable, self-cleaning, transparent, and moisture/oxygen-barrier coating films for food packaging†

Vu Thi Tuyet Thuy, ‡[a,b] Lam Tan Hao, ‡[a,b] Hyeonyeol Jeon, [a]
Jun Mo Koo, [a] Jaeduk Park,[c] Eun Seong Lee, [c] Sung Yeon Hwang, *[a,b]
Sejin Choi, *[a] Jeyoung Park *[a,b] and Dongyeop X. Oh *[a,b]

Plastic packaging effectively protects food from mechanical, microbial, and chemical damage; however, oxygen and moisture permeate these plastics and spoil the food. Thus, the gas barrier function is usually imparted through metallic or halogenated polymeric coatings. However, the former blocks visible light, while the latter causes environmental concerns. Moreover, plastic packaging contaminated with food scraps and stains requires a washing process for recycling. To satisfy the key requirements for food packaging, we fabricated a (1) sustainable, (2) self-cleaning, (3) transparent, and (4) oxygen/moisture barrier coating on poly(ethylene terephthalate) (PET) film. A spray-assisted layer-by-layer assembly of negatively charged cellulose nanofibers and positively charged chitosan nanowhiskers was coated on one side of the PET film. Salt bridge-mediated synergistic interplay between these highly crystalline nanomaterials imparted a low oxygen transmission rate of less than $0.1 \text{ mL m}^{-2} \text{ day}^{-1}$. The other side of the PET film was formed with a porous surface by spray-coating of silica nanoparticles and chitosan nanowhiskers. Thereafter, the porous surface was impregnated with bio-based sunflower oil. This side repelled the contaminants and exhibited a low water vapor transmission rate of $1.4 \text{ g m}^{-2} \text{ day}^{-1}$. The gas barrier performance meets the packaging requirements for most food products. This coating has high potential for sustainable packaging applications.

Introduction

Plastics have become an indispensable part of our lives. As a result, annual plastic production has reached 380 million tons.[1–3] Plastic films such as those made of poly(ethylene terephthalate) (PET), nylon, and polyethylene are ideal packaging materials as their viscoelasticity protects the product against tolerable mechanical shocks, and they are generally resistant

[a]*Research Center for Bio-Based Chemistry, Korea Research Institute of Chemical Technology (KRICT), Ulsan 44429, Republic of Korea. E-mail: crew75@krict.re.kr, schoi@krict.re.kr, jypark@krict.re.kr, dongyeop@krict.re.kr*
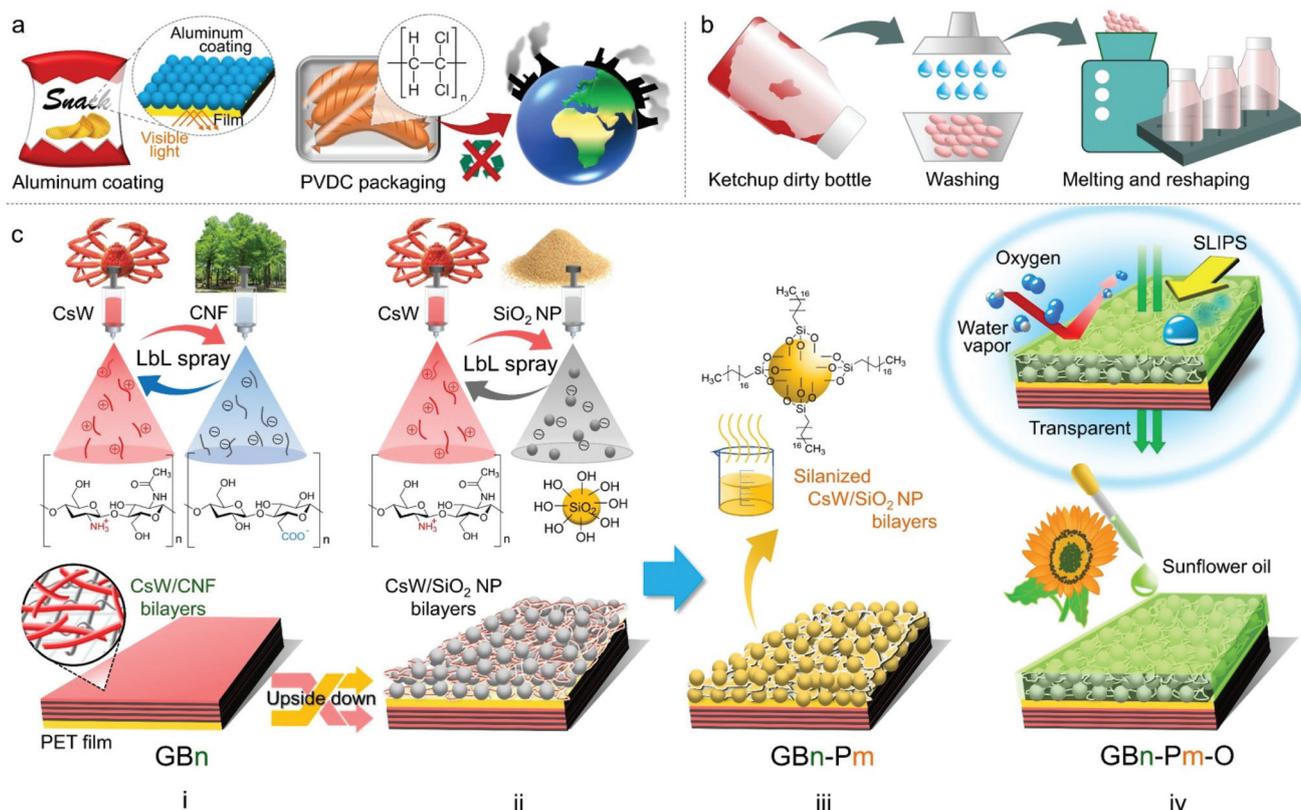[b]*Advanced Materials and Chemical Engineering, University of Science and Technology (UST), Daejeon 34113, Republic of Korea*
[c]*Department of Biomedical Chemical Engineering, The Catholic University of Korea, Bucheon-si 14662, Gyeonggi-do, Republic of Korea*

†Electronic supplementary information (ESI) available: Additional data including sizes and surface features of nanomaterials, transparency, ATR-FTIR spectra, OTR *vs.* relative humidity, UV-Vis spectra and contact angles before and after oil infusion, SEM images and water sliding angles after mechanical abrasion, and cytotoxicity and cell attachment; supporting Movies. See DOI: 10.1039/d0gc03647a
‡These authors contributed equally.

to microorganisms and chemical damage.[4–6] The largest market for plastics is the food packaging industry, whose growth was recently accelerated by a global shift from reusable to single-use containers, relieving the concerns of pandemics such as COVID-19.[7] Out of the total plastic waste generated worldwide, approximately 9% is recycled, 12% is incinerated, and the rest are discarded through landfills.[1–6]

Functional food packaging has issues related to functional coating layers, and food scraps and stains (Fig. 1a and b). First, food packaging has functional coating layers in addition to plastic films. Plastics are mostly permeable to oxygen and moisture and thus fail to prevent quality losses owing to oxidation or hydration/dehydration. To improve the oxygen or moisture barrier properties, coatings consisting of metals and chlorinated polymers, such as poly(vinyl chloride) (PVC) and poly(vinylidene chloride) (PVDC), have been applied to plastic films.[8] Aluminum oxide with an oxygen transmission rate (OTR) of approximately $1 \text{ mL m}^{-2} \text{ day}^{-1}$ is most commonly used these days and can effectively store products that require high barriers, such as snacks or coffee ($0.5 \text{ mL m}^{-2} \text{ day}^{-1}$).[9] The metal-coated packaging is opaque; therefore, the contents are not visible. Nanocoatings such as graphene are also con-

Fig. 1 (a) Opacity and environmental issues caused by metal and halogenated polymer-coated gas-barrier films used for food packaging, respectively. (b) Necessary washing process for the recycling of packaging contaminated with food scraps and stains. (c) Fabrication of a sustainable, slippery, transparent, and oxygen/moisture barrier coating on the PET film using naturally abundant cellulose nanofibers (CNFs), chitosan nanowhiskers (CsWs), and silica nanoparticles (SiO$_2$ NPs). (i) (CsW/CNF)$_n$-based gas barrier coating *via* spray-assisted LbL assembly on the PET film (GBn). (ii) (CsW/SiO$_2$)$_m$-based porous coating *via* spray-assisted LbL assembly on the other side of the PET film. (iii) Silanization treatment on the porous coating (GBn-Pm). (iv) GBn–Pm infused with sunflower oil (GBn–Pm–O). n and m represent the number of bilayers of (CsW/CNF) and silanized (CsW/SiO$_2$ NP), respectively.

sidered for retaining the original properties of plastic films.[10,11] Nevertheless, these packaging films often give rise to health and environmental issues. The safety of these coating materials to the human body has not been completely explored.[12,13] An emerging approach uses layer-by-layer assembly (LbL) of sustainable materials *via* dip coating on poly(lactic acid) to achieve an all-organic functional packaging.[14,15] However, the dip coating method requires dedication and stringent control to homogenously wet the substrate and obtain the desired deposition of thin films.[16] To recycle the functional packaging film, the coating layer should be delaminated from the film. However, this process incurs heavy expenses. Therefore, most food packaging wastes are disposed of through landfills or incineration. Upon burning, PVDC and PVC release hazardous gases (Fig. 1a).[17]

Second, it is difficult to recycle packaging materials contaminated with food scraps and stains. Therefore, a washing process is required adding to the expenses; hence, recycled plastics from the contaminated packaging lose their price competitiveness (Fig. 1b). In this regard, to prevent fouling on the packaging surface, surfactants or lubricants are often

used. For example, perfluorooctanoic acid is often used in the manufacture of pizza boxes; however, it is subject to regulatory action and voluntary industrial phase-outs owing to health concerns. Therefore, it is necessary to develop next-generation food packaging materials that are (i) sustainable, (ii) transparent, and (iii) self-cleaning, with (iv) oxygen and (v) moisture barrier properties. However, there have been no reports on materials that satisfy all the above conditions at the same time.

To realize this, two references are discussed. In our previous report, which is a reference for barrier properties, the LbL assembly coating of cellulose and chitin nanomaterials achieved a low OTR of less than 0.5 mL m^{-2} day^{-1} owing to the high crystallinity of the bio-nanomaterials.[18] The raw materials used, such as cellulose and chitin, are the most abundant naturally occurring biopolymers.[19–22] They are also renewable and biodegradable.[23–25] The coating is optically transparent due to the ionic interaction-mediated compact assembly between the anionic cellulose and cationic chitin nanomaterials.[18,26,27] However, the bio-nanomaterial coating does not have moisture barrier and self-cleaning properties.[28–32]

The second reference is for a self-cleaning food packaging material, which involves the slippery liquid-infused porous surfaces (SLIPS) technology, first reported by J. Aizenberg *et al.*[33] In brief, a nanotextured porous surface is impregnated with an oily liquid, which is contained in the space stably without leaking.[34–38] As a result, it is superhydrophobic and repels liquid and solid fouling on the surface. However, to ensure this condition, the surface and the repelling liquid of SLIPS are typically composed of inorganic nanomaterials and petrochemical oils, respectively. The lubricant oil must be chemically matched with the substrate to achieve an extremely high affinity.[34,35] The components of SLIPS technology need to be replaced with relatively more environmentally friendly materials. In addition, SLIPS coating does not impart a gas barrier function.

In this study, we report the fabrication of a (1) sustainable, (2) transparent, (3) self-cleaning, and (4) oxygen/moisture barrier film for food packaging (Fig. 1c). For the gas barrier function, the LbL assembly of negatively charged cellulose nanofibers (CNFs) and positively charged chitosan nanowhiskers (CsWs) was coated on one side of the PET film *via* a spray-assisted process [Fig. 1c(i)]. The CNF/CsW multilayer coating significantly reduced the OTR compared with that of the neat PET film, owing to the synergistic interplay between the components within the coating layer. For self-cleaning and moisture barrier properties, a sustainable SLIPS coating was applied on the other side of the PET film. The spray-assisted LbL coating of CsW and modified silica (SiO₂) formed a porous surface [Fig. 1c (ii) and (iii)], which was infused with bio-based sunflower oil

[Fig. 1c(iv)]. This side was slippery and imparted a significantly low water vapor transmission rate (WVTR). In addition, the final product was optically transparent due to the compact assembly of all the constituent building blocks of the coating. The oxygen and moisture barrier performances satisfy the packaging requirements for most food products. The entire coating process is summarized in Movie S1.† Considering the abundance of the naturally occurring raw materials such as cellulose, chitosan, and SiO₂, this coating approach is sustainable and renewable for transparent food packaging.

Results and discussion

The CNFs used in our study were prepared using wood pulp as a cellulose source, which was oxidized in an aqueous solution of sodium hypochlorite at pH 10 with the aid of an oxidant (2,2,6,6-tetramethylpiperidinyloxy radical).[18] Oxidation minimally damages the nanofiber structure and transforms the primary hydroxyl groups on the nanofiber surface into carboxylate groups. Subsequent mechanical disintegration by sonication afforded a stable CNF suspension with a ζ-potential of −44.9 mV at pH 7. The prepared CNFs have a length of 209 ± 74 nm and diameter of 15 ± 3 nm (Fig. 2a, S1, S2, and Table S1†). According to our previous report, CsWs were prepared *via* acid hydrolysis of α-chitin using an aqueous solution of hydrochloric acid, and their surfaces were deacetylated using aqueous NaOH solution.[39] As a result of the rich amino groups present along the backbone of each CsW, they exhibi-
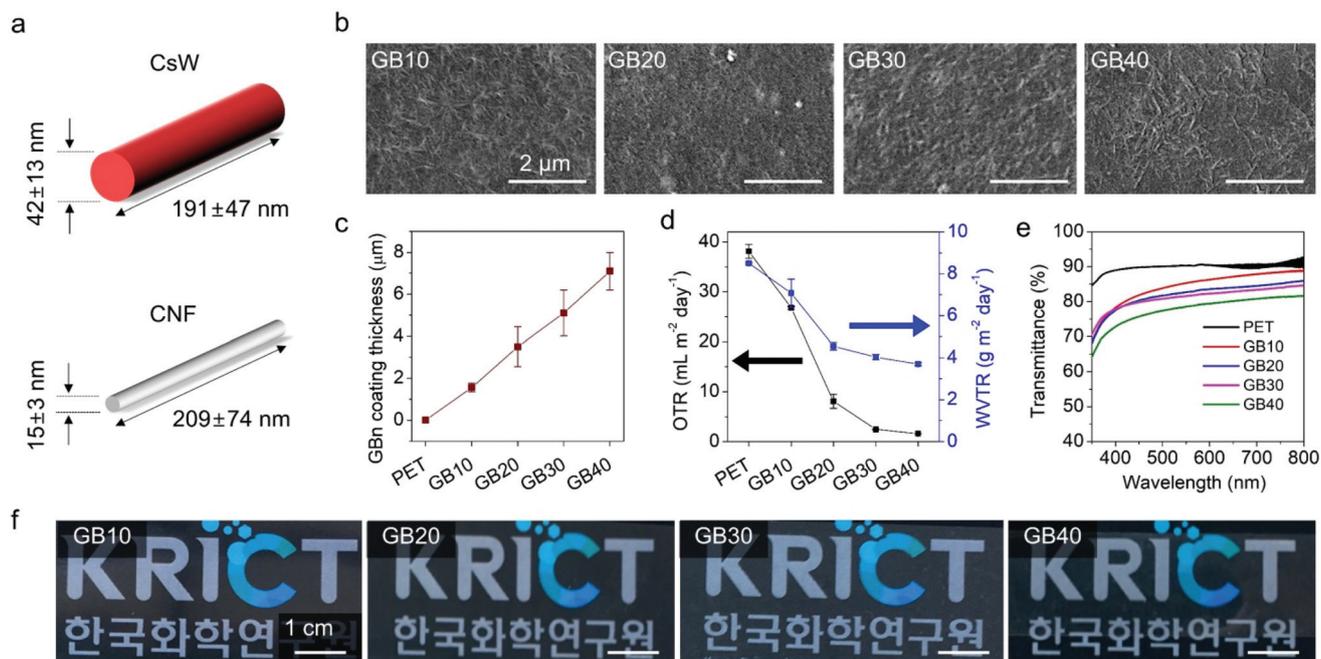

Fig. 2 (a) The representative dimensions of the CsWs and CNFs. (b) SEM images of the GB*n*-coated PET films with different numbers of bilayers. (c) Coating thickness, (d) OTR and WVTR, (e) UV-Vis transmittance spectra, and (f) photographs of 10, 20, 30, and 40 bilayers of (CsW/CNF) LbL coatings on the PET film, labelled as GB10, GB20, GB30, and GB40, respectively.

ted a positive charge with a ζ-potential of +40.3 mV at pH 4, under deposition conditions. The average dimensions of the prepared CsW were 191 ± 47 nm in length and 42 ± 13 nm in diameter (Fig. 2a, S1, S2, and Table S1†). Commercially available spherical SiO_2 nanoparticles (NPs) with an average diameter of 20–30 nm were utilized.

The fundamental coating method employed in this study was the spray-assisted LbL assembly, which has been extensively used as a versatile method to fabricate thin films with controlled architecture and composition.[40–42] LbL assembly is typically achieved by the sequential deposition of oppositely charged components by strong electrostatic interactions.[43–45] Because of its simplicity and versatility, the LbL assembly has rapidly emerged as a platform technique for the construction of hybrid thin-film coatings.[46–48] In this study, for the LbL assembly, we sprayed two oppositely charged aqueous electrolyte solutions on the PET substrate sequentially. The water-based spray coating is an eco-friendly coating. Spray-assisted LbL assembly creates a relatively thicker coating as compared to the more time-consuming immersion-based LbL assembly[49,50] and can achieve coverage over a large area, which makes it one of the most relevant LbL methods for further translation into industrial applications.[51]

The first step of the coating involved the construction of an oxygen barrier, i.e., $(CsW/CNF)_n$ on the PET film [Fig. 1c(i)]. PET films were treated with ultraviolet (UV) light for 20 min on both sides. The UV irradiation of the PET film resulted in the scission of the C–O and C–C bonds and the production of free radicals and hydrophilic moieties such as hydroxyl and carboxyl bearing partial negative charges (Fig. S3†).[52,53] Thus, the first coating layer, i.e., positively charged CsWs, adhered strongly to the UV-treated PET surface via NH_3^+-mediated charge–dipole and cation–π interactions. Following the introduction of the first layer, the opposite electrical charges and the different aspect ratios of CsWs and CNFs led to the formation of subsequent tightly bonded layers, resulting in a stable coating with excellent barrier properties. The aqueous solutions of 0.1 wt% CNF and 0.1 wt% CsW were sequentially sprayed at 80 °C, and the resulting film was then hot pressed. The $(CsW/CNF)_n$ bilayer coating is coded as GBn, where GB and n represent the gas barrier and the number of bilayers, respectively. The bilayers were stacked up to 40 layers (GB40), that is, $(CsW/CNF)_{40}$. Fig. 2b reveals that the PET film was homogeneously coated with the

CsW/CNF assembly, and the CsWs and CNFs were closely packed together. The thickness of the multilayer film of $(CsW/CNF)_n$ was determined by scanning electron microscopy (SEM) images of the cross-section. The thickness increased linearly with respect to the number of bilayers, suggesting a nanoscale blending of the respective components within the multilayer. The average thickness of a single bilayer was approximately 170 nm. The thickness of GB40 was approximately 7 μm (Fig. 2c and Table S2†). In addition to compactness, the GB coating exhibited appreciable stability against finger rubbing (Fig. S4†), and the integrity of the coating was robust against strong mechanical bending and one-year aging.[18]

We then investigated the effect of the coating thickness on the OTR, WVTR, and transparency (Fig. 2d–f and Table S2†). The control sample, a bare PET substrate, exhibited OTR and WVTR values of 38.1 mL m^{-2} day^{-1} and 8.5 g m^{-2} day^{-1}, respectively. Upon coating with $(CsW/CNF)_n$, the OTR and WVTR values of the PET films decreased sharply to 1.6 mL m^{-2} day^{-1} and 3.7 g m^{-2} day^{-1}, respectively, for GB40 (Fig. 2d). Moreover, the difference in their respective dimensions aided in forming tight networks in which the larger CNFs provided a rigid framework, and the smaller CsWs filled the local defects within the CNF meshes, such as holes and voids. This enhanced oxygen barrier performance was almost saturated to 2.45 mL m^{-2} day^{-1} for 30 bilayers because of the intrinsic limitation of fibrous CNF and CsW materials. Despite such an intrinsic limitation, the OTR of the (CsW/CNF) coating was found to be as low as that of a 40 nm-thick Al coating on the PET film.[54,55]

The oxygen permeability is not only determined by the nature of the coating materials but also depends on the relative humidity (RH).[56] As a representative, the OTR dependence of the GB40 film on RH was investigated and is presented in Fig. S5 and Table S3.† The oxygen barrier of the film at 30 and 60% RH was less than 5 mL m^{-2} day^{-1}, not significantly different from the OTR under dry conditions. When the RH was 90%, the OTR of the GB40 film increased to just below 10 mL m^{-2} day^{-1}, comparable with that of the GB20 film and nearly four-fold lower than that of the bare PET at 0% RH (Fig. S5a†). Several orders of magnitude increase in OTR at a high RH is typical behaviour of hydrophilic polymers because water absorption can expand the gap between the polymer chains and provide additional passage for oxygen. However, the OTR values of the GB40 film are maintained within one order of magnitude at elevated humidity, much lower than in other biopolymers[57] and comparable with that of many commercially benchmarked petroleum-based polymers.[8]

The outstanding oxygen barrier performance of the GB40 film can be attributed to the surface chemistry of the nanomaterials and the effect of hot pressing. A combination of heat and compression can induce additional interfacial bonding between nanomaterials and restrict their movement, thereby reducing water penetration.[18,58] The stable reading of OTR values at high humidity within 24 h confirms that water vapours could not be absorbed further into the coating layer (Fig. S5b†). These results suggest the significant practical relevance of the film over a large humidity range (up to 60%). Even at a higher RH, its performance is sufficient for the storage of several fresh foods, which do not normally require a very low OTR (Fig. 4e). However, it is necessary to improve the WVTR value because it is still high for products requiring extremely low moisture transmission.

The transparency of the GBn-coated PET film gradually decreased with an increase in the number of bilayers, as confirmed by the ultraviolet–visible (UV-Vis) light transmittance and photographic images (Fig. 2e, f and S6†). Nevertheless, a high transmittance of more than 78.5% at 550 nm was obtained for the GB40 film. Notably, the transparency of the

GB20 film was approximately 85% at 550 nm. Moreover, it is worth noting that the transparency reduction induced by the GB coating is significantly lower than that induced by the inorganic gas barrier coatings of graphene derivatives[59,60] and aluminum.[61]

The second step of coating involved the construction of a porous structure on the PET film [Fig. 1c(ii)]. The GB40 film was turned upside down and spray-coated with the (CsW/SiO$_2$ NP)$_m$ LbL coating. The aqueous suspensions of 0.1 wt% CsW and 2 wt% SiO$_2$ NPs were sequentially deposited on the surface at 80 °C. Thereafter, the (CsW/SiO$_2$ NP) coating was silanized with trichloro(octadecyl)silane fumes in a chamber [Fig. 1c(iii) and S7†]. The resulting silanized (CsW/SiO$_2$ NP) bilayer coating is denoted as Pm, where P and m represent the porous surface and the number of bilayers, respectively. The bilayers were stacked up to P4, that is, (CsW/SiO$_2$ NP)$_4$. In other words, GB40–P1, GB40–P2, GB40–P3, and GB40–P4 films were prepared. The thickness of Pm gradually increased from 0.9 μm (P1) to 7.1 μm (P4) with an increase in the number of P bilayers (Fig. 3c). The SEM images present the porous structure of the GB40-Pm films (Fig. 3a). The surface morphology of Pm contrasts with that of GBn. GBn exhibited a compact structure with no porosity owing to the opposite charges and a common high aspect ratio of CNFs and CsWs. Meanwhile, the interaction between CsW and SiO$_2$ NPs occurs mainly *via* van der Waals forces and hydrogen bonding with poor ionic attraction because the surface of SiO$_2$ NPs possesses weak negative charges. In addition, the SiO$_2$ NPs have a spherical shape, in contrast to the rod shape of CsW. As a result, the Pm side exhibited a highly porous structure and an uneven surface. The water contact angle of the GB40–Pm film increased to 154° at m = 4 with an increase in the number of P bilayers (Fig. 3b). The silanized SiO$_2$ NPs induced a hydrophobic surface. The hydrophobic and porous structures can absorb oil well. The third step was to fill the nano-porous structure with sunflower oil. The vertically laid GB40-Pm film was filled with sunflower oil for 2 h and then centrifuged at 1000 rpm for 1 min to remove the excess lubricant, producing GB40–Pm–O (O stands for the oiled surface). To verify the successful infusion of sunflower oil onto the CsW/SiO$_2$ NP porous surface, UV-Vis spectroscopy was carried out (Fig. S8a†). All the GB40–Pm–O films exhibited a higher transmittance than the GB40–Pm films within the 400–800 nm range. This is because the voids in the (CsW/SiO$_2$ NP) coating were filled with sunflower oil, which reduced the surface reflection of the bare PET film.[62] In addition, the oil infusion resulted in decreased surface roughness, as indicated by the reduction in the water contact angle of all films from >150° to ~90° (Fig. S8c†).

The self-cleaning ability of the GB40–Pm–O coating was evaluated by the water sliding angle (Fig. 3d), which is a function of water repellence. The GB40–P0 sample, that is, the silanized bare PET surface, exhibited a water sliding angle of 60°. The P coating decreased the water sliding angle of the PET film to 20° (P2–4). After oil infusion, the sliding angles of all the GB40–Pm–O coatings were below 5°, allowing the water droplets to slide readily when the surface was tilted slightly.
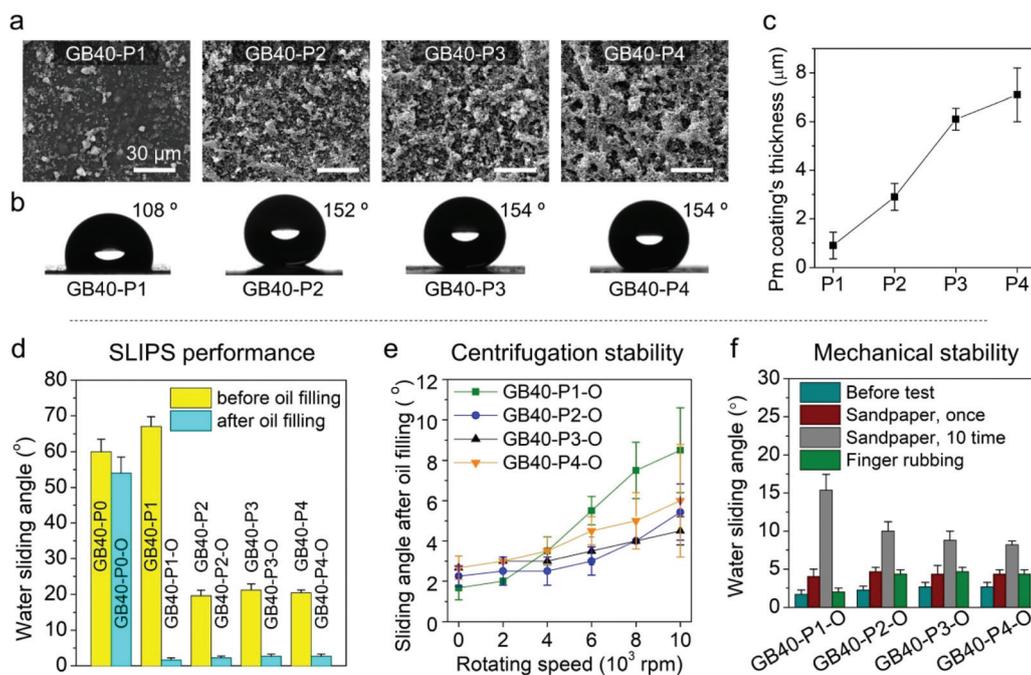
Fig. 3 (a) SEM images, (b) contact angle data, and (c) thickness of the Pm coating, where Pm denotes the silanized (CsW/SiO$_2$ NP)$_m$ bilayer coating on the other side of the GP40 film. Subsequently, GB40–Pm was then infused with sunflower oil and denoted as GB40–Pm–O. (d) Water sliding angles of the GB40–Pm *vs.* GB40–Pm–O samples before and after oil filling. Water sliding angles of the GB40–Pm–O sample after (e) centrifugation and (f) mechanical abrasion tests.

The coatings were wetted by sunflower oil, which eliminated the pinning points and created a slippery repellent surface for water.[62] The water repellence of the coatings mainly depends on the stability of the lubricant film.[62,63] Hence, the mechanical resistance of the coating was investigated (Fig. 3e and f).[64] The substrates were subjected to mechanical shear stress induced by centrifugation at different rotational speeds. After centrifugation at 4000 rpm, all the GB40–Pm–O coatings displayed a sliding angle of less than 5°, and after 10 000 rpm, they still retained a water sliding angle of less than 10° (Fig. 3e and Movie S2†). At high rotating speeds, the minimum sliding angles of the GB40–P3–O and GB40–P4–O coatings were larger than those of the GB40–P2–O coating, probably because the $(CsW/SiO_2\ NP)_3$ and $(CsW/SiO_2\ NP)_4$ coatings have a higher number of pinning points as compared to the $(CsW/SiO_2\ NP)_2$ coating owing to the longer deposition time. When all the GB40–Pm–O films were strongly rubbed with a finger, they exhibited a sliding angle of less than 5°. The SEM images of the porous surface after manual handling and strong rubbing support this minute damage (Fig. S9a and b†). As a much stronger abrasion stress, a piece of sandpaper was placed on the surface under a weight of 1 kg and then dragged to cause surface damage. After a single sandpaper treatment, all the GB40–Pm–O films displayed a sliding angle of less than 5°.

After 10 such sandpaper treatments, the GB40–P2–O, GB40–P3–O, and GB40–P4–O coatings exhibited sliding angles of less than 10° (Fig. 3f and Movie S3†). In addition to mechanical impact, the stability and performance of the SLIPS coating may also depend on the packed content, especially when the content is oil absorbing. Therefore, the self-cleaning ability of the GB40–P2–O film was investigated. The film surface was exposed to potato chips by vigorous shaking for 15 min and left at room temperature for 24 h. After exposure to the oil-absorbing chips, the GB40–P2–O still exhibited a considerable water repellence at a sliding angle of 6° (Movie S4†). We speculate that the sub-micro porosity of the $(CsW/SiO_2\ NP)$ coating exhibited more favourable interactions with sunflower oil than with the oil-absorbing chips; thus most of the oil was retained on the SLIPS surface. Together, the data suggest that this self-cleaning coating is stable to a considerable extent.

The merits of the GB40–P2–O coating are summarized in Fig. 4. The GB40–P2–O coating exhibited a relatively high light transmittance of 85% at 550 nm (Fig. 4a, b and S8†). Interestingly, the GB40–P2–O film presented a higher light transmittance (more transparent) than the GB40 film, although the former was thicker than the latter. It also exhibited a low OTR of less than 0.1 mL m^{-2} day^{-1}, which is below the measurement limit of the OTR tester (Fig. 4c). Its WVTR at
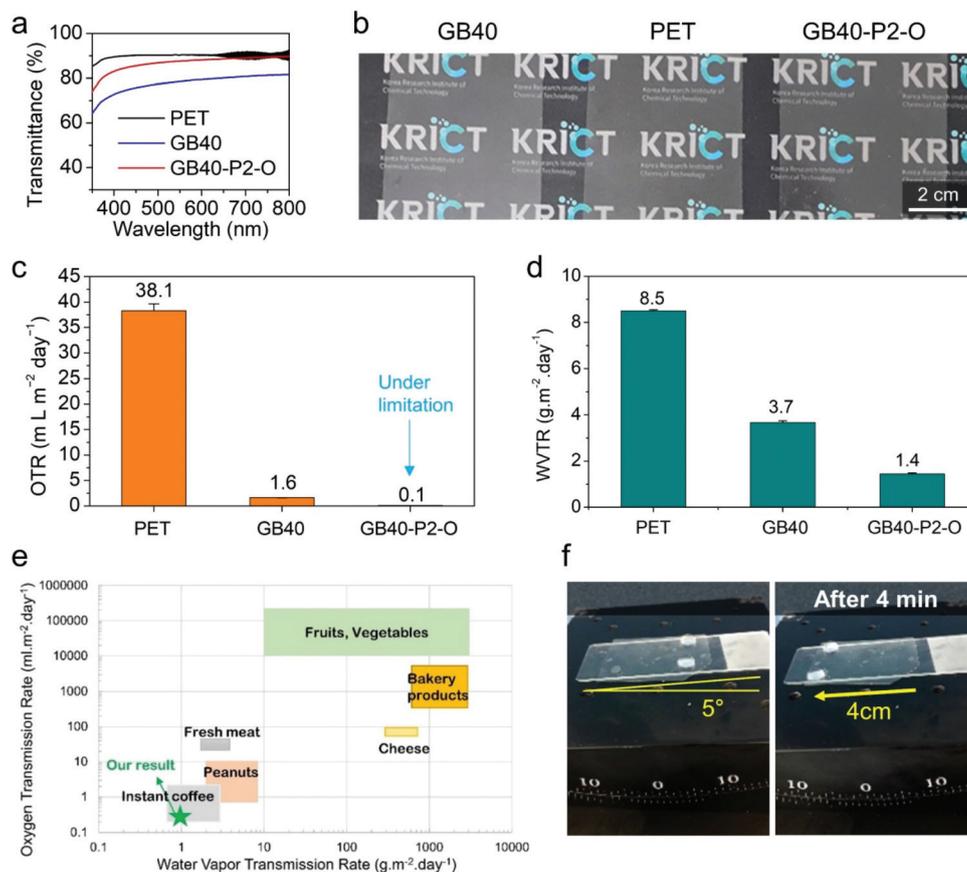

Fig. 4 (a) UV-Vis light transmittance spectra, (b) photographs, (c) OTR, and (d) WVTR of the PET, GB40, and GB40–P2–O samples. (e) The OTR and WVTR requirements of packaging for different foods. (f) Water repellent properties of the GB40–P2–O sample.
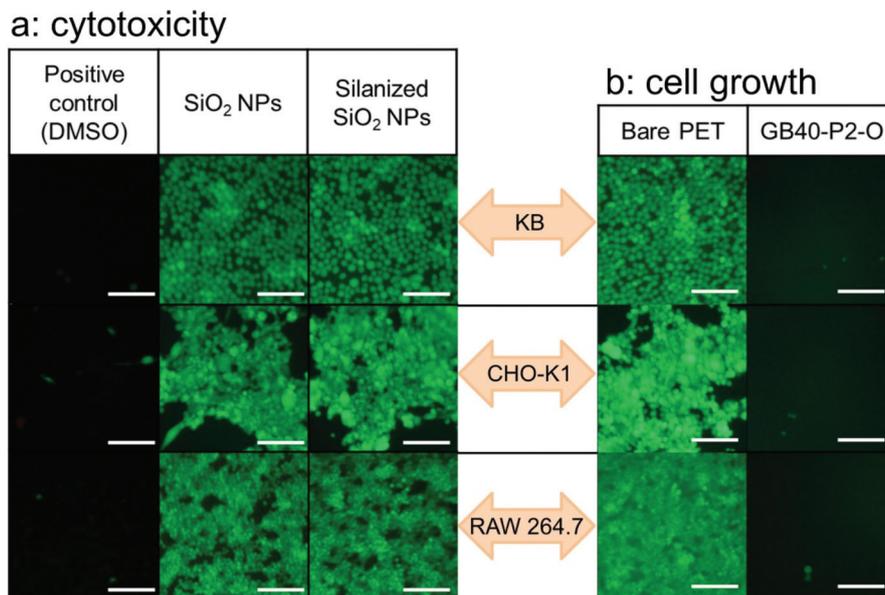
Fig. 5 Confocal images of different types of cells treated with FDA/EB solution to identify live cells (green): (a) cytotoxicity test of the bare SiO$_2$ and silanized SiO$_2$ NPs, and (b) cell growth on the bare PET and SLIPS–coated films (scale bar: 100 μm).

50% RH and 23 °C reduced dramatically from 8.5 g m^{-2} day^{-1} to approximately 1.4 g m^{-2} day^{-1} owing to the hydrophobic layer being filled with the lubricant oil (Fig. 4d). Notably, the oxygen and moisture barrier performance meet the packaging requirements for most food products, including highly oxidation-sensitive foods, such as coffee beans (Fig. 4e).[65,66] The SLIPS coating side displayed excellent self-cleaning performance at 5°, and with various aqueous liquids and oil-in-water emulsions such as beer, milk, ketchup, mayonnaise (80% oil), and ink (Fig. 4f and Movie S5†).

In addition, fundamental cytotoxicity and cell culture experiments were carried out because this coating film was prepared for use as a food packaging material. To investigate the cytotoxicity of the bare SiO$_2$ and silanized NPs on cell growth, the cells (human epidermoid carcinoma KB, Chinese hamster ovary normal CHO-K1, and mouse macrophage normal RAW 264.7) were incubated with each NP sample for 24 h. All the NP samples exhibited negligible cell cytotoxicity. In the fluorescein diacetate (FDA)/ethidium bromide (EB) cell staining test, green fluorescence (indicating live cells) was observed due to the chemical transformation of the FDA dye in live cells. On the other hand, red fluorescence (dead cells) generated by the EB dye was not observed, indicating the non-cytotoxicity of the NP samples (Fig. 5a and S10†). In addition, the number of cells growing on the surface of the GB40–P2–O film was significantly lower than those on the bare PET film (Fig. 5b and S11†), indicating that the cell adhesion properties of the sunflower oil-infused (CsW/SiO$_2$)-coated PET film were significantly low, probably due to their surface fluidity.[67,68] The result suggests the antifouling of harmful microorganisms in food packaging films in future.

Conclusions

In conclusion, we developed an advanced food packaging material with oxygen/moisture barrier and self-cleaning properties by combining cellulose, chitosan, and SiO$_2$ nanomaterials. The LbL deposition of crystalline CNFs and CsWs decreased the OTR because of the strong electrostatic attraction and differences in the aspect ratio between the nanomaterials minimized the void defects. The other side of the film was subjected to a self-cleaning technology called SLIPS using sustainable nanomaterials (SiO$_2$ NPs and CsW) to create a porous structure infused with bio-based sunflower oil. The self-cleaning surface endured mechanical stresses such as sandpaper rubbing quite well. The resultant films were highly transparent owing to the tight assembly of the CNFs and CsWs and a full infusion of the porous surface without any remaining void. The functional films fabricated in this study not only satisfied food storage conditions in terms of providing oxygen and moisture barriers but also exhibited attractive functions such as food packaging, transparency, and self-cleaning properties. In addition, all the components are abundantly available and renewable. This study opens a new approach for the development of future food packaging materials that integrate properties such as high transparency, excellent barrier, and self-cleaning.

Experimental

Materials

PET films (average thickness of 50 μm) were provided by SKC (Suwon, South Korea). Both sides of the PET film were UV-

treated for 20 min before coating. Trichloro(octadecyl)silane, SiO_2 NPs and chitin were purchased from Sigma-Aldrich (St. Louis, MO, USA) and used without further purification. CNFs were purchased from the University of Maine (USA), and they had a surface COO^- content of 1.4 mmol g^{-1}. Sunflower oil was purchased from SAJO (Seoul, South Korea). CsWs were synthesized according to our previously reported method.[39] Briefly, 5 g of chitin was first hydrolysed with 150 mL of 3 M HCl aqueous solution under reflux for 3 h at 120 °C. Subsequently, the reaction mixture was washed thoroughly with deionized water, centrifuged, neutralized with a sufficient amount of NaOH, and dialyzed. The resulting product was freeze-dried. Thereafter, 3 g of the dried sample was deacetylated using 200 mL of 30 wt% NaOH aqueous solution under reflux for 6 h at 80 °C. The reaction mixture was then washed thoroughly with deionized water, centrifuged, and neutralized with a sufficient amount of HCl. The resulting neutral CsW suspension was dialyzed against deionized water to remove salt and oligomer byproducts using membranes with a molecular weight cut-off of 10 kDa (Fisher Scientific, USA), and freeze-dried at −40 °C.

Methods

The aqueous solution of CsWs was diluted to 0.1 wt% using distilled water, and its pH was adjusted to 4 using an aqueous solution of 0.1 M HCl. The resulting suspension was ultrasonicated for 5 min at 30% amplitude.

The aqueous solution of CNF was diluted to 0.1 wt% using distilled water, and subsequently, the suspension was ultrasonicated for 5 min at 30% amplitude. SiO_2 NPs were dispersed in distilled water to prepare a 2 wt% suspension, which was ultrasonicated for 5 min at 30% amplitude.

According to our previous study,[18] the LbL coating of CNFs and CsW was performed as described herein. A PET substrate (15 cm × 15 cm) was fixed on a hot plate under vacuum, and the surface temperature was maintained at 80 °C throughout the coating process to evaporate the solvent. Two nozzles, through which the respective CsW and CNF solutions were passed at a rate of 1.0 mL min^{-1}, were employed to spray the solutions on the upper surface of the substrate while moving in a zigzag pattern (50 mm s^{-1}). During the spray-assisted LbL assembly, an additional layer was alternatively deposited onto the surface of the receiving layer, completing a single bilayer structure. For example, the sequential assembly of CsW and CNF afforded a bilayer of $(CsW/CNF)_1$. Finally, PET films coated with the bilayers were subjected to hot-pressing at 80 °C at 32 MPa for 10 min. On the other side of the PET film, CsW (0.1 wt%) and SiO_2 NPs (2 wt%) were also deposited in the same manner. Silanization was carried out by vapor phase deposition of trichloro(octadecyl)silane at 115 °C for 3 h in a closed system, where the (CsW/SiO_2) surface was exposed to silane vapors. For lubrication, the composite film was immersed in sunflower oil for 2 h and then centrifuged at 1000 rpm for 1 min to remove the excess lubricant.

The contact angle was measured using a drop shaped analyzer (DSA-25, Krüss, Hamburg, Germany). The drop volume used for the measurement was 5 μL, and macroscopic images of the droplet were taken with a camera. Sliding angles were measured on a customized tilting angle plate with a droplet volume of 50 μL. All sliding angles were determined at the degree at which the droplet started to move continuously along 4 cm in length without pinning.

The mechanical stability of SLIPS was investigated after dragging sandpaper attached to a weight of 1 kg (or 100, 200 g) on the Pm–O coating with an area of 3 cm × 4 cm (1 to 10 times). The stability of the SLIPS performance was assessed based on the sliding angles of 70 μL sized water droplets.

According to the ASTM 1434-82 standard test method, the OTR was measured using a manometric gas permeation analyzer (Lyssy L100-5000, Systech Illinois Instruments, Thame, UK) at 23 °C and RHs of 0, 30, 60, and 90%. The sample film (10 cm × 10 cm) was affixed to the self-adhesive paper holder provided by Systech Instruments. The sample holder, which separated the upper (pure oxygen) and lower (vacuum) chambers, was inserted into the test chamber. The WVTR was measured according to the ASTM-E90 standard test method using a standard EZ-Cup vapometer (Thwing-Albert, Berlin, Germany) at 23 °C and 50% RH in a humidity chamber equipped with a Temi1300 programmable temperature and humidity controller (Samwon Tech, Gyeonggi-do, South Korea). In detail, 100 g of deionized water was filled into an EZ-cup vapometer, and subsequently, the measured sample, having a circular shape 6.4 cm in diameter, was quickly sealed with a threaded ring flange between the two neoprene gaskets and placed in the chamber, preset at 23 °C and 50% RH. WVTR was calculated from the weight loss of water for a specific time and over the area of the cup opening. The thickness of the LbL coating was measured from the SEM images of the cross-sections of the pristine and LbL-coated PET films. Transmittance experiments of the films were performed on a UV-Vis spectrometer (UV-2600, Shimadzu Corp., Kyoto, Japan) at a resolution of 0.5 nm. Fourier transform infrared (FT-IR) spectra were recorded on a Nicolet iS50 FT-IR spectrometer (Thermo Fisher Scientific, Waltham, USA) equipped with an attenuated total reflection (ATR) mode on a diamond/ZnSe crystal. The scanning range was between 4000 and 650 cm^{-1} at a resolution of 4 cm^{-1}, and the number of scans was 128.

To verify the cytotoxicity of each NP sample (sterilized with 70 wt% ethanol), the cell viability of KB, CHO-K1, and RAW 264.7 cells incubated with each NP sample was measured. All cells were obtained from the Korea Cell Line Bank and cultured in Dulbecco's modified Eagle's medium or Roswell Park Memorial Institute-1640 medium containing each sample, 10 wt% fetal bovine serum, and 1 wt% penicillin/streptomycin at 36.5 °C for 24 h under a 5% CO_2 atmosphere. Dimethyl sulfoxide (DMSO, 5 wt%) was used as a positive control. Cell viability was evaluated using a Cell Counting Kit-8 (CCK-8, Dojindo, Inc., Rockville, MD, USA). The data of quintuplicate samples ($n = 5$) were expressed as the mean ± standard deviation. All data were evaluated using Student's t-test at a significance level of $p < 0.01$ (**). In addition, the treated cells were stained

using FDA (10 μg mL^{-1})/EB (40 μg mL^{-1}) solution (phosphate buffered saline, pH 7.4) for 5 min at 37 °C to identify live cells.

Conflicts of interest

There are no conflicts to declare.

Acknowledgements

Notes and references

1 R. Geyer, J. R. Jambeck and K. L. Law, *Sci. Adv.*, 2017, **3**, e1700782.
2 S. B. Borrelle, J. Ringma, K. L. Law, C. C. Monnahan, L. Lebreton, A. McGivern, E. Murphy, J. Jambeck, G. H. Leonard, M. A. Hilleary, M. Eriksen, H. P. Possingham, H. De Frond, L. R. Gerber, B. Polidoro, A. Tahir, M. Bernard, N. Mallos, M. Barnes and C. M. Rochman, *Science*, 2020, **369**, 1515–1518.
3 R. A. Sheldon and M. Norton, *Green Chem.*, 2020, **22**, 6310–6322.
4 O. Horodytska, F. J. Valdés and A. Fullana, *Waste Manage.*, 2018, **77**, 413–425.
5 F. Degli Innocenti and T. Breton, *ACS Sustainable Chem. Eng.*, 2020, **8**, 9239–9249.
6 M. Rabnawaz, I. Wyman, R. Auras and S. Cheng, *Green Chem.*, 2017, **19**, 4737–4753.
7 J. C. Prata, A. L. P. Silva, T. R. Walker, A. C. Duarte and T. Rocha-Santos, *Environ. Sci. Technol.*, 2020, **54**, 7760–7765.
8 J. Lange and Y. Wyser, *Packag. Technol. Sci.*, 2003, **16**, 149–158.
9 C. F. Struller, P. J. Kelly and N. J. Copeland, *Surf. Coat. Technol.*, 2014, **241**, 130–137.
10 B. M. Yoo, H. J. Shin, H. W. Yoon and H. B. Park, *J. Appl. Polym. Sci.*, 2014, **131**, 39628.
11 D. Pierleoni, Z. Y. Xia, M. Christian, S. Ligi, M. Minelli, V. Morandi, F. Doghieri and V. Palermo, *Carbon*, 2016, **96**, 503–512.
12 B. Fadeel, C. Bussy, S. Merino, E. Vázquez, E. Flahaut, F. Mouchet, L. Evariste, L. Gauthier, A. J. Koivisto, U. Vogel, C. Martín, L. G. Delogu, T. Buerki-Thurnherr, P. Wick, D. Beloin-Saint-Pierre, R. Hischier, M. Pelin, F. Candotto Carniel, M. Tretiach, F. Cesca, F. Benfenati, D. Scaini, L. Ballerini, K. Kostarelos, M. Prato and A. Bianco, *ACS Nano*, 2018, **12**, 10582–10620.
13 A. Sangroniz, J.-B. Zhu, X. Tang, A. Etxeberria, E. Y. X. Chen and H. Sardon, *Nat. Commun.*, 2019, **10**, 3559.
14 T. Zhang, Q. Yu, L. Fang, J. Wang, T. Wu and P. Song, *ACS Appl. Polym. Mater.*, 2019, **1**, 3470–3476.
15 T. Zhang, Q. Yu, J. Wang and T. Wu, *Ind. Eng. Chem. Res.*, 2018, **57**, 4577–4584.
16 D. Grosso, *J. Mater. Chem.*, 2011, **21**, 17033–17038.
17 J. Thornton, *Environmental Impacts of Polyvinyl Chloride Building Materials*, Healthy Building Network, Washington D.C., 2002.
18 T. Kim, T. H. Tran, S. Y. Hwang, J. Park, D. X. Oh and B.-S. Kim, *ACS Nano*, 2019, **13**, 3796–3805.
19 S. Montanari, M. Roumani, L. Heux and M. R. Vignon, *Macromolecules*, 2005, **38**, 1665–1671.
20 T. Saito and A. Isogai, *Biomacromolecules*, 2004, **5**, 1983–1989.
21 J.-B. Zeng, Y.-S. He, S.-L. Li and Y.-Z. Wang, *Biomacromolecules*, 2012, **13**, 1–11.
22 S. Ifuku, R. Nomura, M. Morimoto and H. Saimoto, *Materials*, 2011, **4**, 1417–1425.
23 H. Yu, H.-J. Hong, S. M. Kim, H. C. Ko and H. S. Jeong, *Carbohydr. Polym.*, 2020, **240**, 116348.
24 H. S. Yu, H. Park, T. H. Tran, S. Y. Hwang, K. Na, E. S. Lee, K. T. Oh, D. X. Oh and J. Park, *Pharmaceutics*, 2019, **11**, 258.
25 J.-K. Kim, B. Choi and J. Jin, *Carbohydr. Polym.*, 2020, **249**, 116823.
26 C. C. Satam, C. W. Irvin, A. W. Lang, J. C. R. Jallorina, M. L. Shofner, J. R. Reynolds and J. C. Meredith, *ACS Sustainable Chem. Eng.*, 2018, **6**, 10637–10644.
27 H.-L. Nguyen, Z. Hanif, S.-A. Park, B. G. Choi, T. H. Tran, D. S. Hwang, J. Park, S. Y. Hwang and D. X. Oh, *Polymers*, 2018, **10**, 501.
28 C. Aulin, M. Gällstedt and T. Lindström, *Cellulose*, 2010, **17**, 559–574.
29 A. Ferrer, L. Pal and M. Hubbe, *Ind. Crops Prod.*, 2017, **95**, 574–582.
30 H. Fukuzumi, T. Saito, T. Iwata, Y. Kumamoto and A. Isogai, *Biomacromolecules*, 2009, **10**, 162–165.
31 J. Wu, K. Zhang, N. Girouard and J. C. Meredith, *Biomacromolecules*, 2014, **15**, 4614–4620.
32 J. M. Morrissette, P. J. Carroll, I. S. Bayer, J. Qin, D. Waldroup and C. M. Megaridis, *Green Chem.*, 2018, **20**, 5169–5178.
33 T.-S. Wong, S. H. Kang, S. K. Y. Tang, E. J. Smythe, B. D. Hatton, A. Grinthal and J. Aizenberg, *Nature*, 2011, **477**, 443–447.
34 C. Howell, T. L. Vu, C. P. Johnson, X. Hou, O. Ahanotu, J. Alvarenga, D. C. Leslie, O. Uzun, A. Waterhouse, P. Kim, M. Super, M. Aizenberg, D. E. Ingber and J. Aizenberg, *Chem. Mater.*, 2015, **27**, 1792–1800.
35 K. Manabe, T. Matsubayashi, M. Tenjimbayashi, T. Moriya, Y. Tsuge, K.-H. Kyung and S. Shiratori, *ACS Nano*, 2016, **10**, 9387–9396.
36 K. Han, L. Heng, Y. Zhang, Y. Liu and L. Jiang, *Adv. Sci.*, 2019, **6**, 1801231.

37 G. H. Zhu, S.-H. Cho, H. Zhang, M. Zhao and N. S. Zacharia, *Langmuir*, 2018, **34**, 4722–4731.

38 L. Xiao, J. Li, S. Mieszkin, A. Di Fino, A. S. Clare, M. E. Callow, J. A. Callow, M. Grunze, A. Rosenhahn and P. A. Levkin, *ACS Appl. Mater. Interfaces*, 2013, **5**, 10074–10080.

39 T. H. Tran, H. L. Nguyen, D. S. Hwang, J. Y. Lee, H. G. Cha, J. M. Koo, S. Y. Hwang, J. Park and D. X. Oh, *Carbohydr. Polym.*, 2019, **205**, 392–400.

40 C. Sung, K. Hearn, D. K. Reid, A. Vidyasagar and J. L. Lutkenhaus, *Langmuir*, 2013, **29**, 8907–8913.

41 F. Carosio, A. Di Blasio, F. Cuttica, J. Alongi, A. Frache and G. Malucelli, *Ind. Eng. Chem. Res.*, 2013, **52**, 9544–9550.

42 Y. Wang, Z. Li, Y. Li, J. Wang, X. Liu, T. Song, X. Yang and J. Hao, *ACS Appl. Mater. Interfaces*, 2018, **10**, 10490–10500.

43 Z. Tang, Y. Wang, P. Podsiadlo and N. A. Kotov, *Adv. Mater.*, 2006, **18**, 3203–3224.

44 T. Zhang, L. Fang, N. Lin, J. Wang, Y. Wang, T. Wu and P. Song, *Green Chem.*, 2019, **21**, 5405–5413.

45 G. Laufer, C. Kirkland, A. A. Cain and J. C. Grunlan, *ACS Appl. Mater. Interfaces*, 2012, **4**, 1643–1649.

46 J. J. Richardson, J. Cui, M. Björnmalm, J. A. Braunger, H. Ejima and F. Caruso, *Chem. Rev.*, 2016, **116**, 14828–14867.

47 K. Ariga, Y. Yamauchi, G. Rydzek, Q. Ji, Y. Yonamine, K. C.-W. Wu and J. P. Hill, *Chem. Lett.*, 2014, **43**, 36–68.

48 M. A. Priolo, D. Gamboa, K. M. Holder and J. C. Grunlan, *Nano Lett.*, 2010, **10**, 4970–4974.

49 A. Izquierdo, S. S. Ono, J. C. Voegel, P. Schaaf and G. Decher, *Langmuir*, 2005, **21**, 7558–7567.

50 Y. Li, X. Wang and J. Sun, *Chem. Soc. Rev.*, 2012, **41**, 5998–6009.

51 G. M. Nogueira, D. Banerjee, R. E. Cohen and M. F. Rubner, *Langmuir*, 2011, **27**, 7860–7867.

52 L. Hou, S. Bi, H. Zhao, Y. Xu, Y. Mu and Y. Lu, *Appl. Surf. Sci.*, 2017, **403**, 248–259.

53 P. Falkenstein, D. Gräsing, P. Bielytskyi, W. Zimmermann, J. Matysik, R. Wei and C. Song, *Front. Microbiol.*, 2020, **28**, 689.

54 E. H. H. Jamieson and A. H. Windle, *J. Mater. Sci.*, 1983, **18**, 64–80.

55 V. R. Tobin, H. Suttle and H. E. Assender, *Thin Solid Films*, 2017, **642**, 142–150.

56 A. Tayeb, M. Tajvidi and D. Bousfield, *Sustainable Chem.*, 2020, **1**, 198–208.

57 N. Lavoine, I. Desloges, A. Dufresne and J. Bras, *Carbohydr. Polym.*, 2012, **90**, 735–764.

58 M. Österberg, J. Vartiainen, J. Lucenius, U. Hippi, J. Seppälä, R. Serimaa and J. Laine, *ACS Appl. Mater. Interfaces*, 2013, **5**, 4640–4647.

59 J. Heo, M. Choi and J. Hong, *Sci. Rep.*, 2019, **9**, 2754.

60 J. Weber, V. Calado and M. Van De Sanden, *Appl. Phys. Lett.*, 2010, **97**, 091904.

61 G. Hass and J. E. Waylonis, *J. Opt. Soc. Am.*, 1961, **51**, 719–722.

62 N. Vogel, R. A. Belisle, B. Hatton, T.-S. Wong and J. Aizenberg, *Nat. Commun.*, 2013, **4**, 2176.

63 S. Sunny, N. Vogel, C. Howell, T. L. Vu and J. Aizenberg, *Adv. Funct. Mater.*, 2014, **24**, 6658–6667.

64 W. He, P. Liu, J. Jiang, M. Liu, H. Li, J. Zhang, Y. Luo, H.-Y. Cheung and X. Yao, *J. Mater. Chem. A*, 2018, **6**, 4199–4208.

65 M. Nakaya, A. Uedono and A. Hotta, *Coatings*, 2015, **5**, 987–1001.

66 Z. Yu, Y. Ji, V. Bourg, M. Bilgen and J. C. Meredith, *Emergent Mater.*, 2020, **3**, 919–936.

67 U. Manna, N. Raman, M. A. Welsh, Y. M. Zayas-Gonzalez, H. E. Blackwell, S. P. Palecek and D. M. Lynn, *Adv. Funct. Mater.*, 2016, **26**, 3599–3611.

68 N. Keller, J. Bruchmann, T. Sollich, C. Richter, R. Thelen, F. Kotz, T. Schwartz, D. Helmer and B. E. Rapp, *ACS Appl. Mater. Interfaces*, 2019, **11**, 4480–4487.